Pre-exposure to time-restricted feeding reduces tissue CD4$^+$ T cells with limited effect on *Mycobacterium tuberculosis* clearance

Ashish Gupta[1], Nidhi Yadav[1], Ranjan Kumar Nanda[1,*]

[1]Translational Health Group, International Centre for Genetic Engineering and Biotechnology, New Delhi- 110067, India.

Short title: TRF's effect on Mtb clearance

***Corresponding author**:

Ranjan Kumar Nanda,

Translational Health Group, International Centre for Genetic Engineering and Technology, New Delhi-110067, India

Telephone: 91-11-26741358; Email: ranjan@icgeb.res.in

Abstract:

Time-restricted feeding (TRF) in human and animal model systems has been reported to positively impact metabolic health by improving glucose homeostasis and reducing adiposity. However, limited studies have demonstrated its impact on infection conditions like *Mycobacterium tuberculosis*. We subjected 6–8 weeks old male C57BL/6 mice to 8 hr (9 pm to 5 am, lights on/off: 8 am/pm) of TRF for 30 days, and then aerosol infected them with a low dose (100-120 cfu) of *Mycobacterium tuberculosis* (Mtb) H37Rv. We measured tissue mycobacterial burden and $CD4^+$ T-cell distribution at 21 days post-infection (dpi). The TRF mice showed minimal weight gain with better glucose tolerance. In addition, the serum and lung tissue metabolome of TRF and ad-libitum control mice were monitored by using mass spectrometry. The serum and liver metabolome of TRF mice demonstrated perturbation in pathways associated with amino acids and fatty acids. Mtb infection in TRF mice impacted the tyrosine and arachidonic acid metabolism, which may benefit the host. At 21 dpi, the Mtb-infected TRF mice showed tissue (lung, spleen and liver) Mtb load similar to the controls but a significant decrease in the number of $CD3^+$ T cells in the bone marrow and $CD3^+CD4^+$ T cells in the bone marrow and lungs. TRF helps in improving metabolic health, but its effects are lost if it is discontinued.

Keywords: Time-restricted feeding, *Mycobacterium tuberculosis*, metabolomics, immunology

Introduction

Time-restricted eating (TRE) is a traditional practice followed by various civilizations, which primarily restricts the time window of food intake to 4–12 hr a day. Following TRE, overweight, obese and prediabetic individuals lose significant body weight and improve their metabolic status.[1,2] However, the molecular mechanism of TRE and whether it may be useful in the early resolution of infectious disease conditions like TB is unknown.

In time-restricted feeding (TRF), mice were provided access to food during the lights-off phase to align food availability with the expression of metabolic enzymes, as they are nocturnal animals.[3,4] TRF in mice improved metabolic health by aligning food availability with the expression of enzymes responsible for nutrient utilization, reducing fat mass, dampening high-fat diet-induced weight increase, improving glucose homeostasis, and reducing inflammation.[2,3,5] Although various studies in mice have demonstrated that TRF reduces inflammation and lowers inflammatory cytokines and chemokine expression, limited reports show its impact on the immune system.[2,6–10]

In this study, we aimed to investigate the effect of TRF for 30 days on the immune system in C57BL/6 and whether it helps in containing *Mycobacterium tuberculosis* (Mtb) H37Rv infection. Male C57BL/6 mice were subjected to 30 days of TRF followed by aerosol infection with Mtb. We assessed the serum and liver metabolome after 30 days of TRF and again after 21 days post infection (dpi). We also assessed immune cell distribution at 21 dpi. With widespread adoption of TRF, understanding the role of TRF to improve cellular or tissue level metabolism and whether it could benefit the host in resolving infection will be critical.

Methodology

Ethical statement: In this study, all the experiments were performed following the approved procedures of the Institutional Animal Ethics Committee of the International Centre for Genetic Engineering and Biotechnology, New Delhi (ICGEB/IAEC/16072024/41.8).

Study Animals: Six–eight-weeks male C57BL/6 mice were housed 5 animals per cage under a 12 hr light-/dark cycle. Mice were randomly assigned to an ad libitum (ALF) or a time-restricted feeding group (TRF). Mice in the TRF group had access to the food only for 9 hr from Zeitgeber time (ZT)13–ZT21, where ZT0 is the time when the lights are switched on and ZT12 is the time when the lights are switched off. Food intake and body weight were monitored daily and weekly, respectively, for the entire experiment duration. Mice were euthanized by isoflurane overdose, followed by cervical dislocation. Tissues (lungs, spleen, liver and bone marrow) were isolated to assess tissue mycobacterial burden and immune cell distribution.

Intraperitoneal glucose tolerance test (iPGTT): After fasting the mice for 16 hr (5 am to 9 pm), glucose (1 g/kg body weight) was introduced through i.p. and blood glucose levels were measured from the tail vein at different intervals (0, 15, 30, 60, 90 and 120 min) using a glucometer (Dr. Morepen BG-03 Gluco One Glucometer). Whole blood samples were collected via retro-orbital bleeding from mice after 16 hr of fasting and stored at room temperature for 20 minutes. Whole blood was centrifuged at 3500 g for 20 min at 4°C to separate serum. The harvested serum was aliquoted and stored at -80°C for further analysis.

Serum insulin and free fatty acid measurement: Fasting insulin levels were measured in the serum of mice undergone 16 hours of fasting, using a Rat/Mouse Insulin ELISA kit from Millipore Sigma (Cat no. EZRMI-13K) following the manufacturer's instructions. Fasting-free fatty acid levels in the serum of experimental mice were measured using a fluorometric assay (Cayman Chemical, Cat no. 700310) following the manufacturer's instructions.

Homeostatic model assessment of insulin resistance (HOMA-IR): HOMA-IR was calculated using the following formula[11]:

$$\text{HOMA-IR} = \frac{Insulin\ (\mu\text{IU ml}^{-1}) \times Fasting\ glucose\ (mmol\ l^{-1})}{22.5}$$

Metabolite isolation: To the serum (100 µl), chilled methanol (400 µl) and internal standard (ribitol, 2 µl, 0.5 mg/ml) were added and vortexed before incubating at -20°C overnight. These samples were centrifuged at 16,000 g for 10 min at 4°C, and the supernatant was collected and dried in a SpeedVac. The dried pellet was resuspended in 5% acetonitrile and transferred to an autosampler vial for liquid-chromatography mass spectrometry (LC-MS) data acquisition. The LC-MS acquired data were preprocessed using Compound Discoverer 3.3 for metadata preparation, and to identify deregulated metabolites and pathways, MetaboAnalyst 6.0 was used. Similarly, to the liver (50 mg) tissue chilled with 80% methanol (400 µl), internal standard (ribitol) and zirconium beads (2 mm, 250 mg) were added and homogenized with three cycles (30 s on; 30 s off) using Biospec Mini-Beadbeater-16. After bead beating, samples were incubated on ice for 30 min, then centrifuged at 16,000 g for 10 min at 4°C. The supernatant was collected and dried in a SpeedVac. We incubated the dried pellet with methoxamine hydrochloride (2%, 40 µl) at 60°C for 2 hours at 900 rpm in a thermomixer. After the incubation, N-methyl-N-(trimethylsilyl)trifluoroacetamide (MSTFA, 70 µl) was added and incubated at 60°C for 30 minutes at 900 rpm in a thermomixer. After incubation, the samples were centrifuged at 10,000 g for 10 minutes at 25°C and the supernatant was transferred to gas chromatography (GC) vial inserts for GC-MS analysis using a 7890 Gas Chromatograph coupled to a Pegasus 4D GC×GC- time-of-flight mass spectrometer. The GC-MS data were analyzed using ChromaTOF and MetaboAnalyst 6.0 to identify the deregulated metabolites and pathways.

Mtb H37Rv infection: A set of mice undergoing TRF and ALF for 30 days were aerosol infected with a low dose (100-120 cfu) of Mtb H37Rv using a Madison chamber in the

tuberculosis aerosol challenge facility in the host institute. Mice were humanely euthanized on day 1 and 21 post-infection to monitor tissue bacterial burden. Mice tissues (lung, spleen, and liver) were aseptically collected and homogenized in phosphate-buffered saline, and the tissue homogenates were plated on 7H11 agar plates supplemented with PANTA. The plates were incubated at 37°C in a humidified incubator for 21 days, and colonies were enumerated to calculate the colony-forming units (CFUs).

Tissue immune cell phenotyping: Harvested tissues (lungs, spleen) of experimental mice groups were incubated with collagenase D (1 µg/mL) and DNase I (0.5 mg/mL) in RPMI 1640 medium at 37 ºC for 30 min. The cell suspension was passed through a cell strainer (70 µm) and centrifuged at 400 × g at 4 ºC for 5 min. The cell pellet was lysed with RBC cell lysis buffer at room temperature for 5 min. After washing the immune cells with PBS, the cells were stained for surface markers. For immune cell isolation from bone marrow, epiphyses of the femur and tibia were cut with scissors, and they were placed in a 0.6 ml microcentrifuge tube (MCT) and kept in a separate tube. After centrifuging at 2000 rpm for 5 sec, the cell pellet was collected, and after resuspending in RPMI 1640, the medium was again centrifuged. The pellet was resuspended in RBC cell lysis buffer after incubating for 5 min at room temperature, and the cells were washed with PBS before staining with viability dye (LIVE/DEAD™ Fixable Near-IR Dead Cell Stain) and surface markers (CD3-FITC and CD4-BV785) on ice for 30 min. After washing, the cells were with PBS and resuspended in FACS buffer (0.5% FBS in PBS) before data acquisition using BD LSRFortessa X-20, and data were analyzed using FCS Express Version 6.0.

Data analysis: All group-specific data were presented as mean ± standard error of the mean (sem). Mann Whitney/Welch's t-test was used to compare statistical significance between the two groups, and a p-value<0.05 at a 95% confidence interval was considered statistically

significant. The plots were generated using GraphPad Prism Version 8 or R package "ggplot2".

Results

TRF influences body weight gain and impacts host glucose homeostasis: To monitor the effect of TRF on the host, 6–8 weeks C57BL/6J mice were subjected to TRF regimen with access to food for 8 h from ZT13 to ZT21 whereas the control *ad libitium* (ALF) group had unrestricted access to the same amount of food (Figure 1A). The TRF group consumed the same amount of food as the ALF group (Figure 1B) and, in the initial two weeks, lost 1.5% body weight (Figure 1B). After 30 days of TRF, the mice lost 5.49% of body weight, whereas the ALF control group gained 16.62% (Figure 1C). At weeks 1 and 2, mice undergoing TRF lost significant body weight compared to the ad-libitum controls (Supplementary Figure S1A).

On day 14, the TRF group had a significantly lower area under the curve for the intraperitoneal glucose tolerance test, and two-way analysis of variance showed a significant difference between the ALF and TRF group blood glucose levels (Figure 1D). At day 21 and day 28, both the TRF and ALF groups had similar areas under the curve for the intraperitoneal glucose tolerance test, and at 15 minutes post glucose bolus, the TRF group had significantly lower blood glucose levels (Figure 1E and Supplementary Figure S1B). Fasting serum insulin and free fatty acid levels and HOMA-IR were similar at days 15 and 28 between the TRF and ALF mice (Figure F, G, H and I). Initiation of TRF results in significant weight loss at initial time points (up to day 14), but at later time points, body weight becomes similar between the ALF and TRF groups. Similar results in human trials undergoing TRF demonstrated minimal body weight gain and glucose homeostasis.[1]

TRF alters amino acids and fatty acids metabolism: To monitor TRF-induced metabolic alterations in circulation and liver, we performed an untargeted metabolomics experiment (Figure 2A). Principal component analysis (PCA) of the serum metabolome showed slight overlap between the TRF and ALF groups (Figure 2B). We identified 1123 metabolic features in serum, out of which 51 were dysregulated ($\log_2$ fold change $\geq \pm 1.0$; p-value < 0.05) (Supplementary Table S1). These deregulated molecules were involved in different pathways like amino acid (alanine, aspartate, glutamate, arginine, proline, tyrosine) metabolism, lipid (biosynthesis of unsaturated fatty acids, elongation, degradation of fatty acids) metabolism and others like pyrimidine metabolism, and steroid hormone biosynthesis pathways (Figure 2C and D). Serum palmitoleic acid levels were significantly low, and higher cytidine and cystine levels were observed in the TRF groups, indicating an altered fatty acid and pyrimidine metabolism between the study groups. Similarly, global liver metabolome data showed slight overlap in the PCA plot (Figure 2F). Through GC-MS, we captured 119 metabolic features in the liver out of which eight features (propanoic acid, methylmaleic acid, gluconic acid, lysine, benzaldehyde, 10-undecynoic acid, arabinonic acid, and ribonolactone) were dysregulated ($\log_2$ fold change $\geq \pm 1.0$; p-value <0.05) in the TRF mice (Supplementary Table S2). These molecules are involved in the biotin metabolism, propanoate metabolism, pentose phosphate pathway, and lysine degradation pathways, indicating significant differences in the liver metabolism between the TRF and ALF groups (Figures 2G and H). Thus, 30 days of continuous TRF in mice results in significant alterations in amino and fatty acid metabolism at both systemic and tissue levels.

Pre-exposure to TRF minimally affects tissue mycobacterial burden at 21 dpi: To determine whether TRF-induced immune-metabolic changes improve the host's handling of respiratory infections such as tuberculosis, C57BL/6 mice completing 30 days of TRF were aerosol infected with 100–400 CFU of Mtb H37Rv (Figure 3A and Supplementary Figure

S1B). TRF and ALF mice were infected with Mtb and showed decreased body weight irrespective of their dietary status, and similar body weight at 21 dpi (Figure 3B and Supplementary Figure S2B). Post Mtb infection TRF was discontinued and received food *ad libitum*, like the ALF group. Random blood glucose levels between the TRF-TB and ALF-TB groups at 21 dpi were similar (Supplementary Figure S2C). The gross tissue pathology of the TRF-TB and ALF-TB mouse groups showed similar pathology (Figure 3C). At 21 dpi, the Mtb-infected TRF and ALF mice groups had similar lung, spleen and liver tissue mycobacterial burden (Figure 3D). It is important to highlight that post-Mtb infection, both the TRF and ALF groups were subjected to ALF conditions, so the benefit of TRF might be lost in the TRF-TB group. Pre-exposure to TRF did not benefit mice in reducing tissue mycobacterial burden.

Mtb infected mice pre-exposed to TRF showed differential tissue immune cell distribution: The details of the gating strategy adopted to monitor the distribution of $CD3^+$ and $CD4^+$ T cells in multiple tissues (lungs, spleen and bone marrow) of Mtb-infected TRF and ALF mice groups are presented in Figure 3E. The bone marrow of TRF-TB mice had significantly low $CD3^+$ and $CD4^+$ T cells compared to the ALF-TB group (Figure 3F). Similarly, the lung CD4+ T cell population was significantly low in the TRF-TB group (Figure 3G). The splenic $CD3^+$ and $CD4^+$ T cell frequencies were similar between the study groups (Figure 3H). Interestingly, the circulatory IL-α, IFN-γ, and IL-6 levels between Mtb-infected TRF and ALF mice were similar at 21 dpi (Figure 3I). Thus, pre-exposure to TRF resulted in decreased number of $CD3^+$ and $CD4^+$ T cells, key immune cell types for host defence against Mtb, without negatively affecting mycobacterial clearance.

TRF-induced metabolic changes persisted in TRF-TB mice: To determine if TRF-induced metabolic alterations in circulation and liver persist if TRF is discontinued post-Mtb infection, an untargeted metabolomics experiment was attempted. PCA plot of the serum

metabolome showed a clear separation between the TRF-TB and ALF-TB groups (Figure 4A). Out of 1120 metabolite features identified in the serum, 22 metabolic features were dysregulated ($\log_2$ fold change $\geq \pm 1.0$; p-value < 0.05) (Supplementary Table S3). These deregulated metabolites are involved in nicotinate and nicotinamide metabolism, sphingolipid metabolism, fatty acid and steroid hormone biosynthesis (Figure 4B and C). Similarly, global liver metabolome data showed slight overlap in the PCA plot (Figure 4D). We identified 121 metabolic features, out of which 14 were dysregulated ($\log_2$ fold change $\geq \pm 1.0$; p-value <0.05) in the liver of TRF-TB mice (Supplementary Table S4). These molecules were involved in linoleic acid metabolism, fructose and mannose metabolism, galactose metabolism, biosynthesis of unsaturated fatty acids, tyrosine metabolism, amino acid and nucleotide sugar metabolism, and arachidonic metabolism (Figures 4E and F). Thus, alterations induced by TRF in amino acid and fatty acid metabolism persist even after discontinuation.

Discussion

TRF has been demonstrated to prevent weight gain, improve glucose homeostasis, and reduce the size of lipid droplets in mice consuming a high-fat diet (HFD).[2] These effects are achieved despite taking caloric intake primarily by altering the diurnal expression of metabolic genes, i.e., matching food availability with the peak of expression of metabolic enzymes.[17] Although TRF has been demonstrated to have pleiotropic health benefits, extending these benefits to humans has been variable.[12,13]

We observed that TRF for 30 days in C57BL/6 male mice resulted in significant body weight loss in the initial period and loss at later time points. Multiple reports showed mixed findings on the gain or loss of body weight in humans from varied ethnicities adopting TRE for stipulated time periods. Most reports showed minimal body weight loss in humans

undergoing TRE.[1,14–16] Mice receiving HFD following TRF show significantly low body gain compared to ALF controls.[2,17] In our study, mice had access to a normal chow diet in which only 13% of calories are derived from fat, whereas in HFD, fat is responsible for 60% of calories. We observed better glucose homeostasis in TRF mice at an early time (day 15 of TRF), but the effect was abrogated by day 28. During this period, we did not observe any differences in fasting insulin levels or HOMA-IR between the TRF and ALF mice. This could be due to a lack of insulin resistance in 6–8 weeks of male C57BL/6 mice being fed a normal chow diet in contrast to those fed with HFD. TRF has been reported to reduce insulin resistance and improve HOMA-IR levels in diabetic individuals and mice consuming HFD.[1.2] We also did not observe any differences in fasting free fatty acids levels in the serum of TRF mice at days 15 and 28.

TRE in humans is reported to influence pathways associated with amino acids and lipid metabolism.[16] We also observed that TRF remodeled the host metabolome in the circulation and metabolically active liver tissue. Pathways related to amino acid metabolism (alanine, aspartate and glutamate metabolism, arginine and proline metabolism, and tyrosine metabolism), fatty acid metabolism (biosynthesis of unsaturated fatty acids, fatty acid elongation, fatty acid degradation, fatty acid biosynthesis, and steroid hormone biosynthesis) and pyrimidine metabolism were enriched in the circulation of TRF mice post 30 days. Pathways associated with biotin metabolism, propanoate metabolism, pentose phosphate pathway and lysine degradation were enriched in the liver of TRF mice. Fatty acid and amino acid metabolism-related pathways remain altered at 21 dpi.

Caloric restriction (CR) significantly reduced the lung and spleen mycobacterial burden in DBA/2 mice intravenously infected with Mtb H37Rv at 40 dpi.[19] CR in C57BL/6 mice at 40 dpi showed a significant reduction in spleen CFU but no difference in lung CFU with a significant decrease in the IFN-γ levels in the lung homogenate.[19] In our study, TRF and ALF

mice had similar tissue mycobacterial burden (lungs, spleen and bone marrow) at 21 dpi. We assessed tissue mycobacterial burden and immune cell distribution at 21 dpi as the adaptive immune response peaks and the Mtb population reaches a plateau in C57BL/6 mice by 21 dpi.[20] The circulatory pro-inflammatory cytokines (IL-1α, IFN-γ, and IL-6) levels between the study groups were similar. TRF mice had a low $CD3^+$ T cell population in the bone marrow and $CD3^+CD4^+$ T cells in the bone marrow and lungs at 21 dpi.

CR initiated before the Mtb infection resulted in a decreased number of $CD3^+CD4^+$ T cells in the lungs but not in the spleen of intravenously infected with Mtb H37Rv DBA/2 mice at 40 dpi.[19] Differential effect of TRF and CR on tissue mycobacterial burden and immune cell distribution could be explained by differences in the mice strain (C57BL/6 vs DBA/2), differences in timepoints (21 dpi vs 40 dpi), and differences in the mode of infection (aerosol vs intravenous).[19]

A limitation of our study is that we did not assess how TRF affects the functionality of $CD3^+$ or $CD4^+$ T cells or the distribution of other immune cells (such as macrophages and neutrophils) involved in host defense against Mtb. Also, our study did not have either a group in which TRF was continued throughout Mtb infection or initiated after Mtb infection. The inclusion of these groups helped determine if continued TRF or TRF initiated after Mtb infection might have a positive effect on the immune system.

In conclusion, our study showed that TRF remodels host metabolism by altering amino acid and lipid metabolism, and these beneficial effects persist even if TRF is discontinued. However, discontinuing the TRF had no additional effect on mycobacterial clearance at 21 dpi. Pre-exposure to TRF impacted both tissue level metabolism and immune cell ($CD3^+/CD4^+$ T cells) distribution in Mtb-infected mice. Since the decrease in the number of $CD3^+/CD4^+$ T cells did not compromise the host's mycobacterial clearance ability, it

indicates that pre-exposure to TRF might be improving the functionality of $CD3^+/CD4^+$ T cells which needs additional studies.

Acknowledgements

We acknowledge the Department of Biotechnology (DBT), Government of India, for supporting activities through research grants and supporting the Tuberculosis Aerosol Challenge Facility at ICGEB, New Delhi and the ICGEB New Delhi for providing core support to RKN. AG and NY received the Junior Research Fellowship from DBT, Government of India.

Conflicts of Interest: All the authors declare that they have no conflicts of interest.

References

1. Ezpeleta M, Cienfuegos S, Lin S, et al. Time-restricted eating: Watching the clock to treat obesity. Cell Metab. 2024;36(2):301-314. doi:10.1016/j.cmet.2023.12.004
2. Chaix A, Zarrinpar A, Miu P, Panda S. Time-restricted feeding is a preventative and therapeutic intervention against diverse nutritional challenges. Cell Metab. 2014;20(6):991-1005. doi:10.1016/j.cmet.2014.11.001
3. Chaix A, Lin T, Le HD, Chang MW, Panda S. Time-restricted feeding prevents obesity and metabolic syndrome in mice lacking a circadian clock. Cell Metab. 2019;29(2):303-319.e4. doi:10.1016/j.cmet.2018.08.004
4. Regmi P, Chaudhary R, Page AJ, et al. Early or delayed time-restricted feeding prevents metabolic impact of obesity in mice. *J Endocrinol*. 2021;248(1):75-86. doi:10.1530/JOE-20-0404

5. Chaix A, Manoogian ENC, Melkani GC, Panda S. Time-restricted eating to prevent and manage chronic metabolic diseases. Annu Rev Nutr. 2019;39:291-315. doi:10.1146/annurev-nutr-082018-124320
6. Ella K, Sűdy ÁR, Búr Z, et al. Time restricted feeding modifies leukocyte responsiveness and improves inflammation outcome. *Front Immunol*. 2022;13:924541. doi:10.3389/fimmu.2022.924541
7. Turner L, Charrouf R, Martínez-Vizcaíno V, Hutchison A, Heilbronn LK, Fernández-Rodríguez R. The effects of time-restricted eating versus habitual diet on inflammatory cytokines and adipokines in the general adult population: a systematic review with meta-analysis. *Am J Clin Nutr*. 2024;119(1):206-220. doi:10.1016/j.ajcnut.2023.10.009
8. Kim Y, Lee Y, Lee MN, et al. Time-restricted feeding reduces monocyte production by controlling hematopoietic stem and progenitor cells in the bone marrow during obesity. Front Immunol. 2022;13:1054875. doi:10.3389/fimmu.2022.1054875
9. Lee Y, Kim Y, Lee M, Wu D, Pae M. Time-restricted feeding restores obesity-induced alteration in adipose tissue immune cell phenotype. Nutrients. 2021;13(11):3780. doi:10.3390/nu13113780
10. Cissé YM, Borniger JC, Lemanski E, Walker WH 2nd, Nelson RJ. Time-restricted feeding alters the innate immune response to bacterial endotoxin. J Immunol. 2018;200(2):681-687. doi:10.4049/jimmunol.1701136
11. Bowe JE, Franklin ZJ, Hauge-Evans AC, King AJ, Persaud SJ, Jones PM. Metabolic phenotyping guidelines: assessing glucose homeostasis in rodent models. J Endocrinol. 2014;222(3):G13-G25. doi:10.1530/JOE-14-0182

12. Wilkinson MJ, Manoogian ENC, Zadourian A, et al. Ten-hour time-restricted eating reduces weight, blood pressure, and atherogenic lipids in patients with metabolic syndrome. Cell Metab. 2020;31(1):92-104.e5. doi:10.1016/j.cmet.2019.11.004

13. Wei X, Lin B, Huang Y, et al. Effects of time-restricted eating on nonalcoholic fatty liver disease: The TREATY-FLD randomized clinical trial. JAMA Netw Open. 2023;6(3):e233513. doi:10.1001/jamanetworkopen.2023.3513

14. Manoogian ENC, Laferrère B. Time-restricted eating: What we know and where the field is going. Obesity (Silver Spring). 2023;31 Suppl 1(Suppl 1):7-8. doi:10.1002/oby.23672

15. Liu D, Huang Y, Huang C, et al. Calorie restriction with or without time-restricted eating in weight loss. N Engl J Med. 2022;386(16):1495-1504. doi:10.1056/NEJMoa2114833

16. Chang Y, Du T, Zhuang X, Ma G. Time-restricted eating improves health because of energy deficit and circadian rhythm: A systematic review and meta-analysis. iScience. 2024;27(2):109000. doi:10.1016/j.isci.2024.109000

17. Hatori M, Vollmers C, Zarrinpar A, et al. Time-restricted feeding without reducing caloric intake prevents metabolic diseases in mice fed a high-fat diet. Cell Metab. 2012;15(6):848-860. doi:10.1016/j.cmet.2012.04.019

18. Lundell LS, Parr EB, Devlin BL, et al. Time-restricted feeding alters lipid and amino acid metabolite rhythmicity without perturbing clock gene expression. Nat Commun. 2020;11(1):4643. doi:10.1038/s41467-020-18412-w

19. Palma C, La Rocca C, Gigantino V, et al. Caloric restriction promotes immunometabolic reprogramming leading to protection from tuberculosis. Cell Metab. 2021;33(2):300-318.e12. doi:10.1016/j.cmet.2020.12.016

20. Wolf AJ, Desvignes L, Linas B, et al. Initiation of the adaptive immune response to Mycobacterium tuberculosis depends on antigen production in the local lymph node, not the lungs. J Exp Med. 2008;205(1):105-115. doi:10.1084/jem.20071367

Figures

Figure 1. TRF alters glucose homeostasis at early time points does not affect fasting serum insulin and free fatty acid levels. A. Schematic of the experimental design adopted in the study. **B**. Bodyweight with time. **C**. Change in bodyweight with time. **D**. Cumulative food intake per cage in grams. **E**. Intraperitoneal glucose tolerance test at Day 15 and 28 post-TRF. The quantification of the AUC above baseline is shown in the insert. **F**. and **H**. Insulin levels after 16 hr of fasting and corresponding HOMA-IR levels at Day 15 and Day 28, respectively. **G**. and **I**. Free fatty acid levels after 16 hr of fasting at Day 15 and Day 28, respectively. The number of mice analyzed per group for each figure was 5 except B. for which 2 cages per group were analyzed. Each dot represents a biological replicate. Statistical significance was determined using Holm-Sidak method with correction for multiple comparison in **B**. and **C**., two-way repeated-measures ANOVA and Sidak's multiple comparisons tests for ipGTT and unpaired t test with Welch's correction for AUC in **D.** and **E**. and unpaired t test with Welch's correction in **F., G., H. and I.** *$p \leq 0.05$, ***$p \leq 0.001$, ****$p \leq 0.0001$, ns = not significant.

Figure 2. TRF induces metabolism remodeling at both tissue and systemic level. A. Schematic presentation of the method used for metabolite profiling from the TRF and ALF mice serum using LC-MS. **B.** Principal component analysis (PCA) of serum metabolites between the TRF and ALF mice. **C.** Volcano plot showing deregulated metabolites in the serum of the TRF and ALF mice. **D.** Metabolite set enrichment analysis (MSEA) of the deregulated metabolites. **E.** Schematic presentation of the method used for metabolite

profiling from the TRF and ALF mice liver using GC-MS. **F.** PCA of liver metabolites between the TRF and ALF mice. **G.** Volcano plot showing deregulated metabolites in the liver of the TRF and ALF mice. **H.** MSEA of the deregulated metabolites.

Figure 3. TRF decreases CD4+ T cell number in tissue dependent manner at 21 dpi. A. Schematic of experimental design adopted in the study. **B.** Change in bodyweight with time after Mtb infection. **C.** Gross pathology of the lungs, spleen and liver of the ALF and TRF mice. **D.** Mycobacterial burden in the lungs, spleen and liver at 21 dpi. **E.** The gating strategy adopted to determine $CD3^+$ T cells and $CD3^+$ $CD4^+$ T cells. Percentage of $CD3^+$ and $CD3^+$ $CD4^+$ T cells in (**F.**) bone marrow, (**G.**) lungs and (**H.**) spleen. **I.** Levels of pro-inflammatory cytokines IL-1α, IFN-γ and IL-6 in the serum. Each dot represents a biological replicate. Statistical significance was determined using unpaired t test with Welch's correction. **$p \leq 0.01$ and ***$p \leq 0.001$.

Figure 4. TRF induced changes persist at 21 dpi. A. Principal component analysis (PCA) of serum metabolites between the TRF-TB and ALF-TB mice. **B.** Volcano plot showing deregulated metabolites in the serum of the TRF-TB and ALF-TB mice. **C.** Metabolite set enrichment analysis (MSEA) of the deregulated metabolites. **D.** PCA of liver metabolites between the TRF-TB and ALF-TB mice. **E.** Volcano plot showing deregulated metabolites in the liver of the TRF-TB and ALF-TB mice. **F.** MSEA of the deregulated metabolites.

Supplementary figures.

Supplementary Figure S1. TRF decreased body weight and improved glucose homeostasis initially. A. Percentage bodyweight changes at Day 7 and 14 post-TRF. **B.** Intraperitoneal glucose tolerance test at Day 21 post-TRF. The quantification of the AUC above baseline is shown in the insert. Each dot represents a biological replicate. Statistical significance was determined using unpaired t test with Welch's correction in **A.** and two-way

repeated-measures ANOVA and Sidak's multiple comparisons tests for ipGTT and unpaired t test with Welch's correction for AUC in **B.**

Supplementary Figure S2. Relative abundance of different metabolites in the serum.

Supplementary Figure S3. **A.** Lung mycobacterial burden at 1 dpi. **B.** Percentage difference in bodyweight between ALF-TB and TRF-TB mice. **C.** Random blood glucose levels at 21 dpi.

Supplementary Figure S4. Absolute number of $CD3^+$ and $CD3^+CD4^+$ T cells in (**A.**) bone marrow, (**B.**) lungs and (**C.**) spleen at 21 dpi. Each dot represents a biological replicate. Statistical significance was determined using unpaired t test with Welch's correction. *$p \leq 0.05$ and **$p \leq 0.01$.

Figure 1

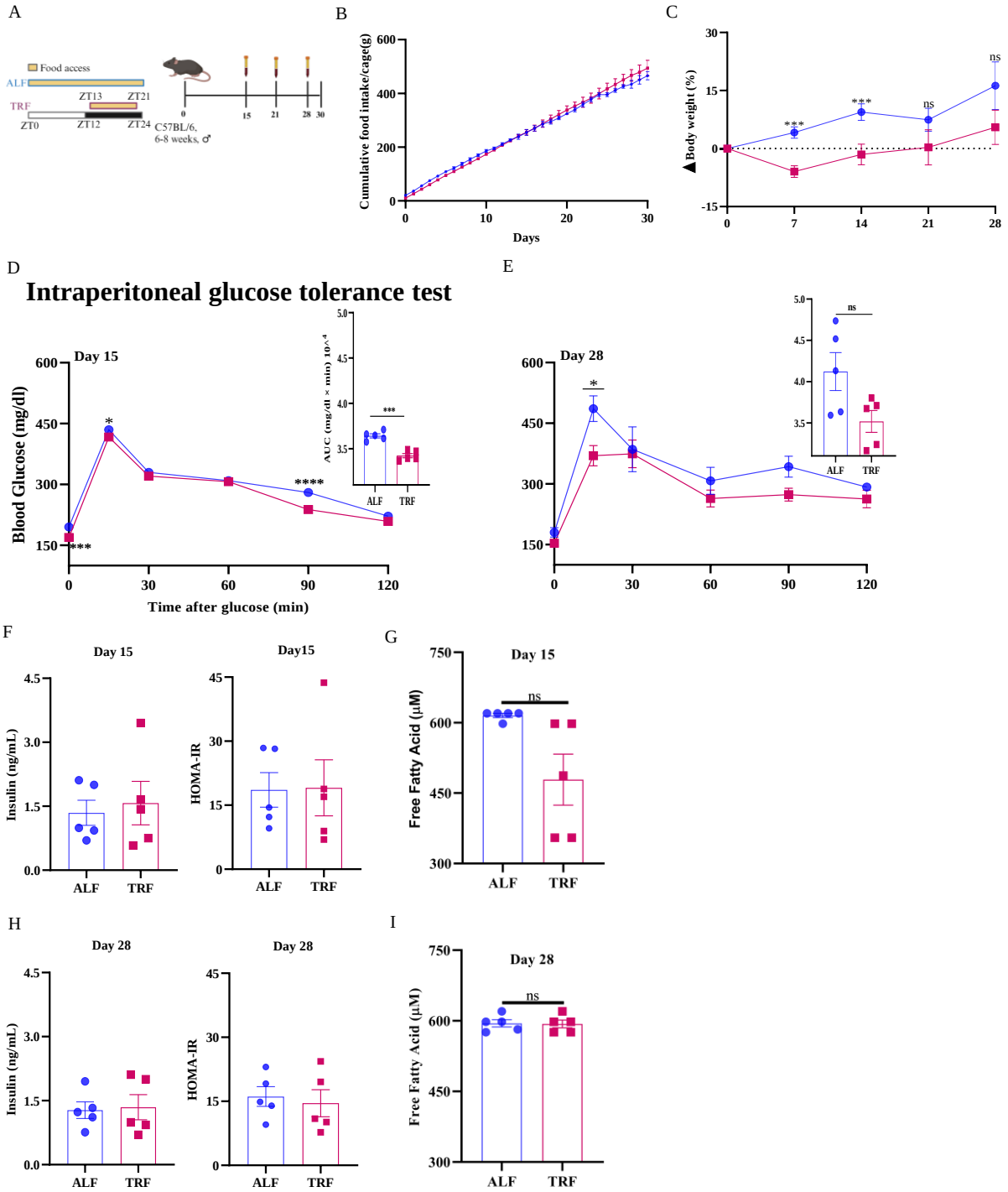
A
Food access
ALF
TRF
ZT13
ZT21
ZT0
ZT12
ZT24
C57BL/6,
6-8 weeks, ♂
0
15
21
28
30
B
Cumulative food intake/cage(g)
Days
C
Body weight (%)
ns
***
D
Intraperitoneal glucose tolerance test
Day 15
Blood Glucose (mg/dl)
Time after glucose (min)
AUC (mg/dl × min) 10^4
ALF
TRF
E
Day 28
F
Day 15
Insulin (ng/mL)
Day15
HOMA-IR
G
Free Fatty Acid (μM)
H
Day 28
I

Figure 2

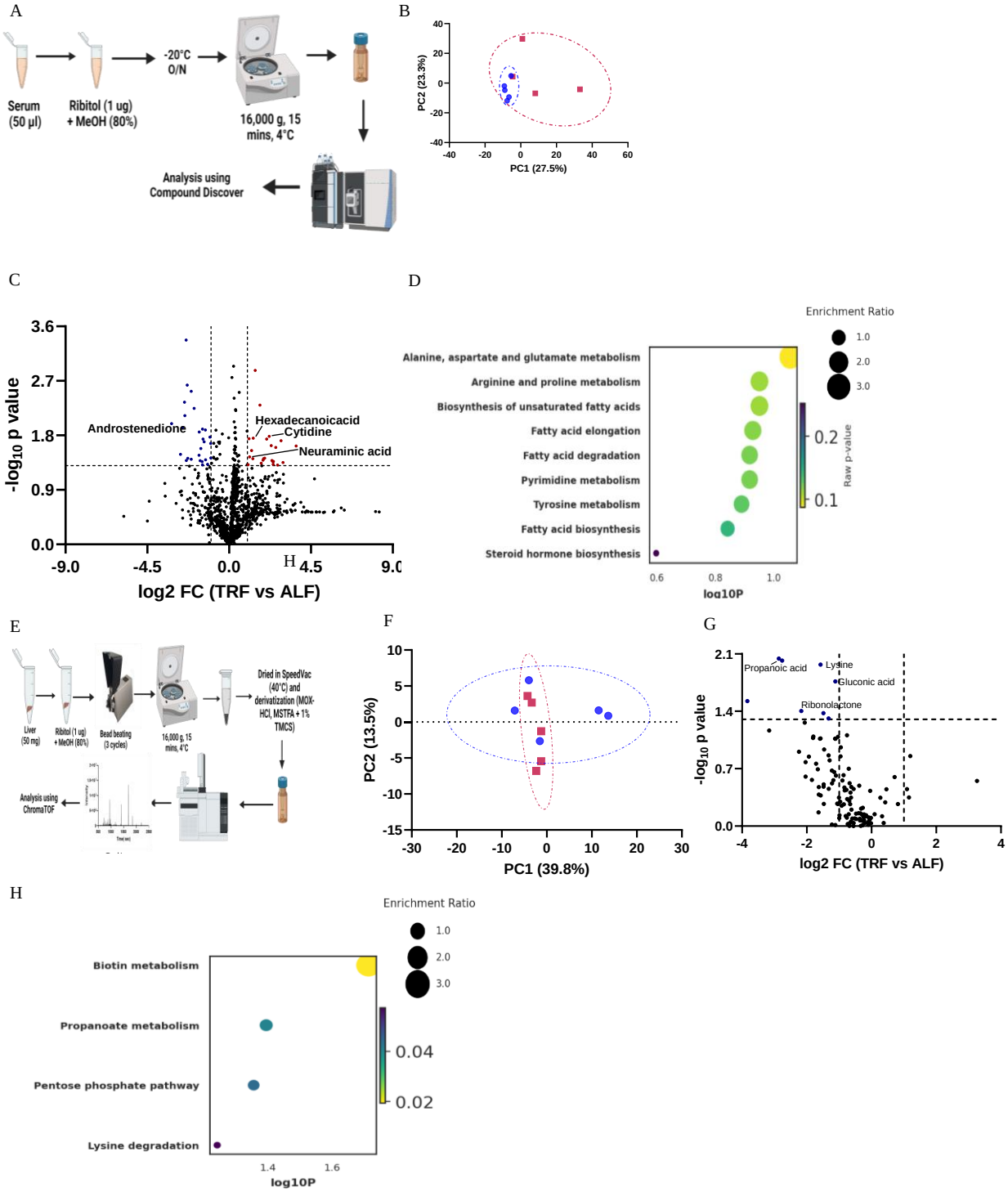
A
Serum (50 µl)
Ribitol (1 ug) + MeOH (80%)
-20°C O/N
16,000 g, 15 mins, 4°C
Analysis using Compound Discover
B
PC2 (23.3%)
PC1 (27.5%)
C
-log10 p value
log2 FC (TRF vs ALF)
Androstenedione
Hexadecanoicacid
Cytidine
Neuraminic acid
D
Enrichment Ratio
Alanine, aspartate and glutamate metabolism
Arginine and proline metabolism
Biosynthesis of unsaturated fatty acids
Fatty acid elongation
Fatty acid degradation
Pyrimidine metabolism
Tyrosine metabolism
Fatty acid biosynthesis
Steroid hormone biosynthesis
Raw p-value
log10P
E
Liver (50 mg)
Ribitol (1 ug) + MeOH (80%)
Bead beating (3 cycles)
16,000 g, 15 mins, 4°C
Dried in SpeedVac (40°C) and derivatization (MOX-HCl, MSTFA + 1% TMCS)
Analysis using ChromaTOF
F
PC2 (13.5%)
PC1 (39.8%)
G
Propanoic acid
Lysine
Gluconic acid
Ribonolactone
-log10 p value
log2 FC (TRF vs ALF)
H
Enrichment Ratio
Biotin metabolism
Propanoate metabolism
Pentose phosphate pathway
Lysine degradation
log10P

Figure 3

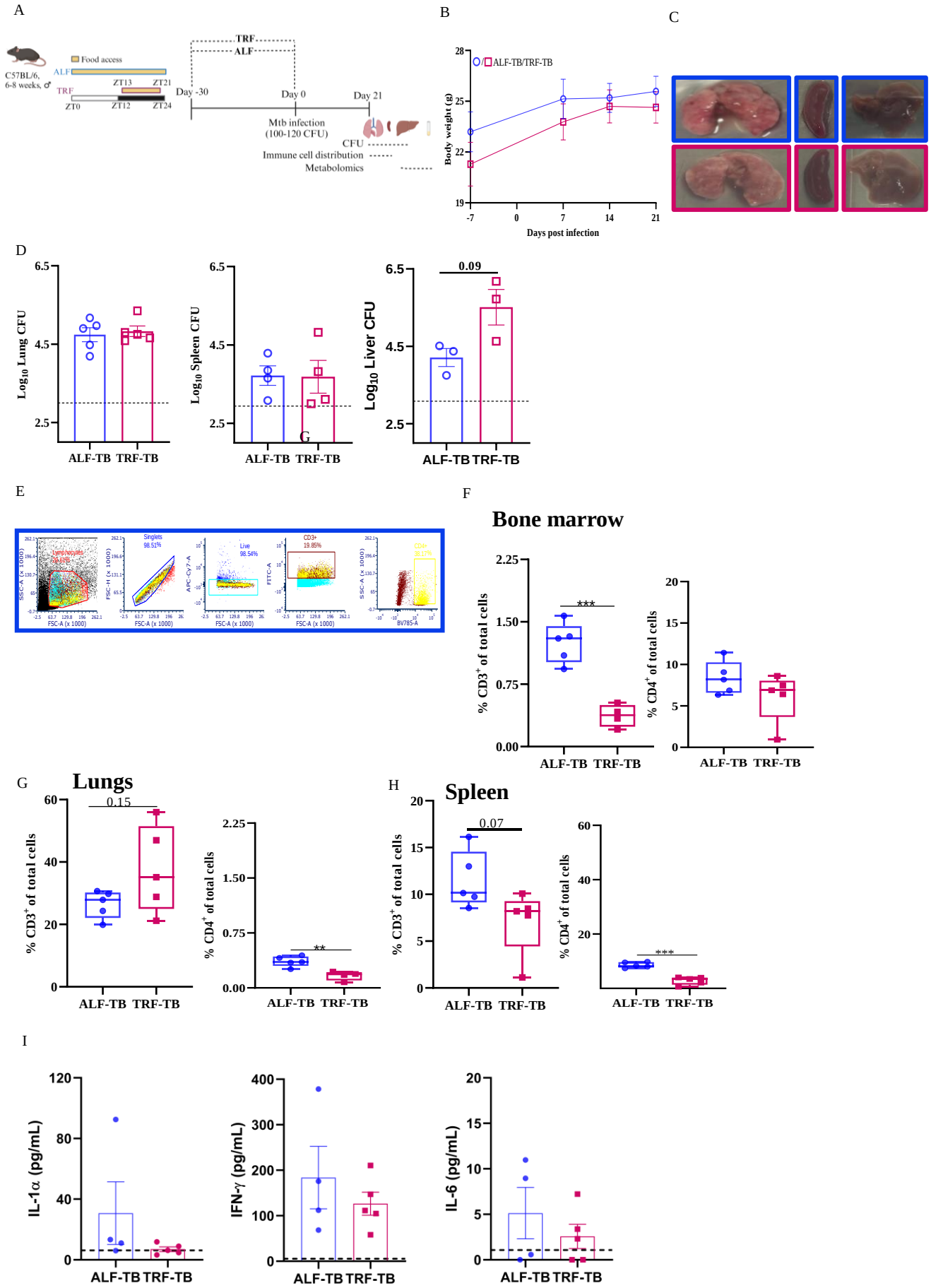
A
Food access
C57BL/6, 6-8 weeks, ♂
ALF
TRF
ZT13
ZT21
ZT0
ZT12
ZT24
TRF
ALF
Day -30
Day 0
Day 21
Mtb infection (100-120 CFU)
CFU
Immune cell distribution
Metabolomics
B
ALF-TB/TRF-TB
Body weight (g)
Days post infection
C
D
Log10 Lung CFU
Log10 Spleen CFU
Log10 Liver CFU
0.09
ALF-TB
TRF-TB
E
Lymphocytes
Singlets 98.51%
Live 98.54%
CD3+ 19.85%
CD4+ 38.17%
FSC-A (x 1000)
SSC-A (x 1000)
FSC-H (x 1000)
APC-Cy7-A
FITC-A
BV785-A
F
Bone marrow
% CD3+ of total cells
% CD4+ of total cells
***
G
Lungs
0.15
**
H
Spleen
0.07
***
I
IL-1α (pg/mL)
IFN-γ (pg/mL)
IL-6 (pg/mL)

Figure 4

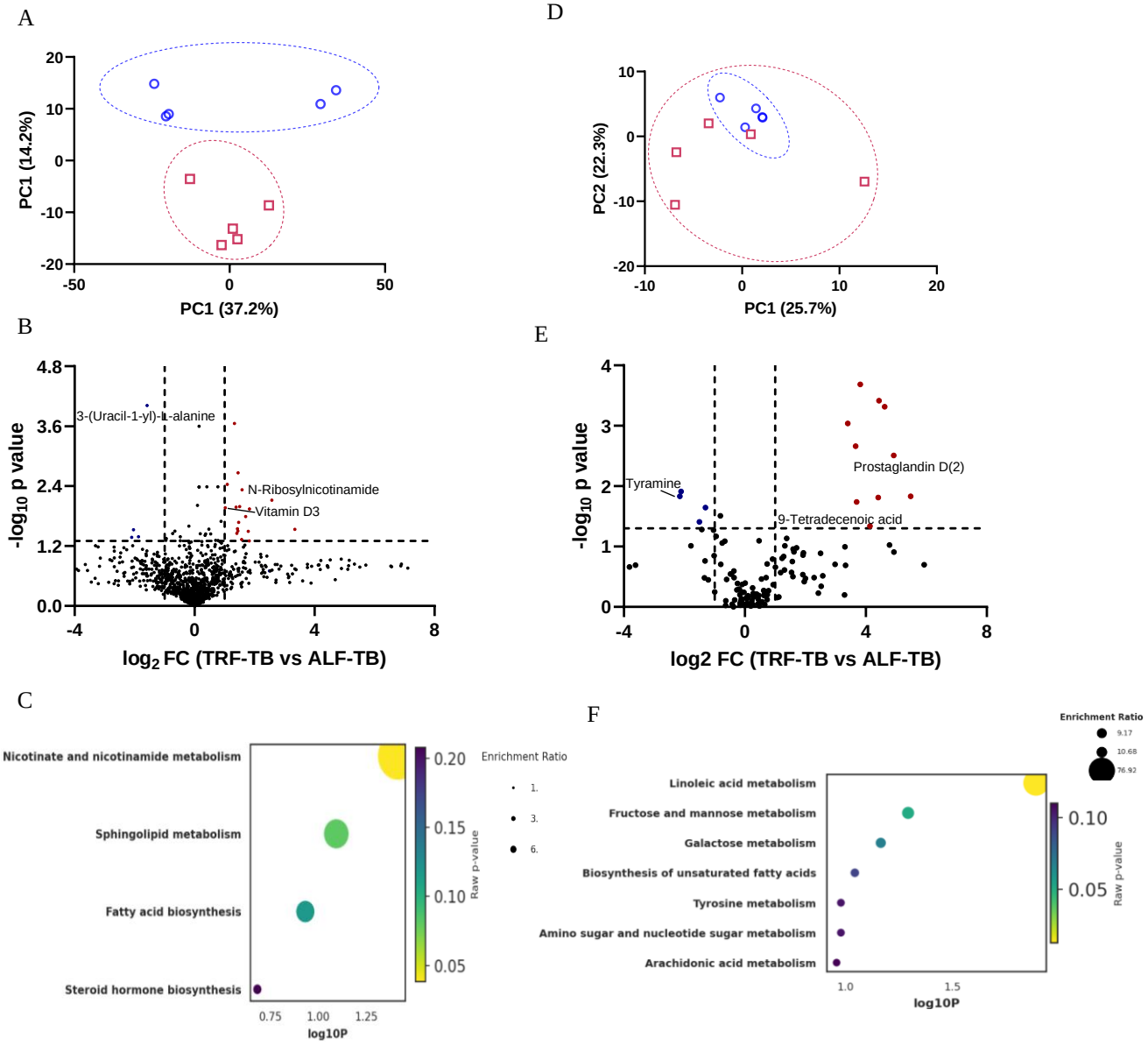
A
PC1 (14.2%)
PC1 (37.2%)
D
PC2 (22.3%)
PC1 (25.7%)
B
-log10 p value
log2 FC (TRF-TB vs ALF-TB)
3-(Uracil-1-yl)-L-alanine
N-Ribosylnicotinamide
Vitamin D3
E
-log10 p value
log2 FC (TRF-TB vs ALF-TB)
Tyramine
Prostaglandin D(2)
9-Tetradecenoic acid
C
Nicotinate and nicotinamide metabolism
Sphingolipid metabolism
Fatty acid biosynthesis
Steroid hormone biosynthesis
log10P
Raw p-value
Enrichment Ratio
F
Linoleic acid metabolism
Fructose and mannose metabolism
Galactose metabolism
Biosynthesis of unsaturated fatty acids
Tyrosine metabolism
Amino sugar and nucleotide sugar metabolism
Arachidonic acid metabolism
log10P
Raw p-value
Enrichment Ratio